FLOW-STRUCTURE INTERACTION NOISE AT LOW MACH NUMBERS

M. S. Howe
Boston University, College of Engineering
110 Cummington Street, Boston MA 02215

SUMMARY

The method of compact Green's functions is described for calculating the sound produced by low Mach number turbulence interacting with a surface and by surfaces in relative motion. The method is very powerful and can supply analytical predictions of complex fluid-structure interaction noise, and can also be used to make acoustic predictions by 'postprocessing' data obtained from a numerical simulation of a hydrodynamic interaction. The theory is illustrated by cases of sound production by a vortex interacting with a sphere, by the linear and nonlinear theories of parallel vortex-airfoil interaction noise, the trailing edge noise produced by an airfoil of finite thickness and of arbitrary chord, and by the compression wave generated when a projectile is fired into a long duct.

1. EQUATION OF VORTEX SOUND

Lighthill's acoustic analogy [1] can be recast to emphasize the importance of vorticity ($\boldsymbol{\omega}$) and entropy fluctuations as sources of sound by taking the *total enthalpy* B to be the fundamental acoustic variable [2, 3]. Lighthill identified the Reynolds stress as the principal acoustic source in homentropic flow. In that case

$$B = \int \frac{dp}{\rho} + \frac{1}{2}v^2,$$

where ρ is fluid density, $p \equiv p(\rho)$ the pressure, and $\mathbf{v}$ denotes velocity, and Lighthill's equation becomes

$$\left(\frac{D}{Dt}\left(\frac{1}{c^2}\frac{D}{Dt}\right) - \frac{1}{\rho}\nabla\cdot(\rho\nabla)\right)B = \frac{1}{\rho}\mathrm{div}(\rho\boldsymbol{\omega}\wedge\mathbf{v}), \tag{1.1}$$

where c is the local speed of sound.

In the irrotational acoustic far field Crocco's form of the momentum equation $\partial\mathbf{v}/\partial t = -\nabla B$ implies that $B = -\partial\varphi/\partial t$, where $\varphi(\mathbf{x},t)$ is the velocity potential that determines the whole motion in the irrotational regions of the fluid. B is therefore *constant* in steady irrotational flow, and at large distances from the sources perturbations in B represent outgoing sound waves. If the mean flow is at rest in the far field, the acoustic pressure $p = \rho_o B \equiv -\rho_o\partial\varphi/\partial t$.

At low Mach numbers M local mean values of ρ and c differ from their uniform respective values ρ_o and c_o by terms of relative order M^2. The vortex sound equation (1.1) can then be simplified (a) by taking $c = c_o$ and $\rho = \rho_o$, and (b) by neglecting nonlinear effects of propagation and the scattering of sound by the vorticity. The production of sound is then governed by

$$\left(\frac{1}{c_o^2}\frac{\partial^2}{\partial t^2} - \nabla^2\right)B = \mathrm{div}(\boldsymbol{\omega}\wedge\mathbf{v}), \tag{1.2}$$

where in the acoustic field

$$p(\mathbf{x},t) \approx \rho_o B(\mathbf{x},t). \tag{1.3}$$

Paper presented at the RTO AVT Symposium on "Ageing Mechanisms and Control: Part A – Developments in Computational Aero- and Hydro-Acoustics", held in Manchester, UK, 8-11 October 2001, and published in RTO-MP-079(I).

2. VORTEX-SURFACE INTERACTION NOISE

Consider the solution of (1.2) in the presence of solid boundaries S that are either stationary or vibrating at small amplitude. Introduce a Green's function $G(\mathbf{x},\mathbf{y},t-\tau)$ that satisfies

$$\left(\frac{1}{c_o^2}\frac{\partial^2}{\partial\tau^2}-\frac{\partial^2}{\partial y_j^2}\right)G=\delta(\mathbf{x}-\mathbf{y})\delta(t-\tau),\quad G=0 \text{ for } \tau>t, \tag{2.1}$$

and has vanishing normal derivatives $\partial G/\partial x_n$, $\partial G/\partial y_n$ respectively for $\mathbf{x}$ and $\mathbf{y}$ on S. Then Green's theorem [3 - 5] supplies the solution of (1.2) in the form

$$B(\mathbf{x},t)\approx-\int(\boldsymbol{\omega}\wedge\mathbf{v})(\mathbf{y},\tau)\cdot\frac{\partial G}{\partial\mathbf{y}}(\mathbf{x},\mathbf{y},t-\tau)d^3\mathbf{y}d\tau+\nu\oint_S\boldsymbol{\omega}(\mathbf{y},\tau)\wedge\frac{\partial G}{\partial\mathbf{y}}(\mathbf{x},\mathbf{y},t-\tau)\cdot d\mathbf{S}(\mathbf{y})d\tau$$

$$+\oint_S G(\mathbf{x},\mathbf{y},t-\tau)\frac{\partial v_j}{\partial\tau}(\mathbf{y},\tau)d\mathrm{S}_j(\mathbf{y})d\tau, \tag{2.2}$$

provided frictional effects on S are effectively the same as for incompressible flow, where ν is the kinematic viscosity, and the vector surface element $d\mathbf{S}$ is directed into the fluid. The first integral describes the production of sound by convecting vorticity. Green's function takes account of the influence of the body on the efficiency of sound production by this source. The second, surface integral represents the sound produced by frictional forces on the body; it can be neglected in most applications at high Reynolds numbers. The final term is the contribution from normal velocity fluctuations on S.

Therefore, at large Reynolds number and for a non-vibrating surface, the pressure in the acoustic far field is given by

$$p(\mathbf{x},t)=-\rho_o\int_V(\boldsymbol{\omega}\wedge\mathbf{v})(\mathbf{y},\tau)\cdot\frac{\partial G}{\partial\mathbf{y}}(\mathbf{x},\mathbf{y},t-\tau)d^3\mathbf{y}d\tau. \tag{2.3}$$

The integral includes contributions from the direct radiation by quadrupole sources within the fluid (with intensity $\propto\rho_o v^3M^5$ per unit volume [1]) and also from dipole sources on S. For a body with surface irregularities comparable in size to the turbulence length scale (when the irregularity is acoustically *compact*) the dipole intensity $\propto\rho_o v^3M^3$; for turbulence near the leading or trailing edge of an airfoil of *non-compact* chord the intensity typically scales like $\rho_o v^3M^2$. Thus at low Mach numbers, compact surface irregularities (or a compact foreign body) and edges of non-compact bodies are usually the dominant sources of flow generated sound. We shall consider these cases separately and demonstrate how detailed acoustic predictions can be made for complex interactions in terms of the appropriate *compact* approximation for the Green's function G.

3. COMPACT BODIES AND COMPACT SURFACE IRREGULARITIES

3.1 Compact bodies and cylindrical bodies of compact cross-section The leading order dipole radiation is calculated by approximating G in (2.3) by the *compact* Green's function [2, 3]

$$G(\mathbf{x},\mathbf{y},t-\tau)=\frac{1}{4\pi|\mathbf{X}-\mathbf{Y}|}\delta\left(t-\tau-\frac{|\mathbf{X}-\mathbf{Y}|}{c_o}\right) \tag{3.1}$$

$$\left.\begin{aligned}\mathbf{X}&=\mathbf{x}-\boldsymbol{\varphi}^*(\mathbf{x})\\ \mathbf{Y}&=\mathbf{y}-\boldsymbol{\varphi}^*(\mathbf{y})\end{aligned}\right\}\text{ Kirchhoff vectors for the body,}$$

where the vector components $X_j(\mathbf{x})$ and $Y_j(\mathbf{y})$ are the velocity potentials of incompressible flow past the body having unit speed in the j-direction at large distances from the body; φ_j^* is the velocity potential of the incompressible flow that would be produced by rigid body motion of S at unit speed in the j-direction. For a cylindrical body of *compact cross-section* parallel to the x_3-direction, we take

$$X_3 = x_3, \quad Y_3 = y_3.$$

The approximation (3.1) represents the solution of (2.1) correct to dipole order provided either $\mathbf{x}$ or $\mathbf{y}$ (or both) lie in the acoustic far field of S, in the limit in which the acoustic wavelength $\lambda \gg \ell \sim$ the length scale of S (Figure 1). Special cases referenced in the illustrations given below are listed in Table 1:

Standard special cases

body	X_1	X_2	X_3
sphere of radius a center at origin	$x_1\left(1+\frac{a^3}{2\lvert\mathbf{x}\rvert^3}\right)$	$x_2\left(1+\frac{a^3}{2\lvert\mathbf{x}\rvert^3}\right)$	$x_3\left(1+\frac{a^3}{2\lvert\mathbf{x}\rvert^3}\right)$
circular cylinder of radius a coaxial with the x_3-axis	$x_1\left(1+\frac{a^2}{x_1^2+x_2^2}\right)$	$x_2\left(1+\frac{a^2}{x_1^2+x_2^2}\right)$	x_3
strip airfoil $-a<x_1<a,\ x_2=0,\ -\infty<x_3<\infty$	x_1	$\mathrm{Re}(-i\sqrt{z^2-a^2})$ $z=x_1+ix_2$	x_3

Table 1

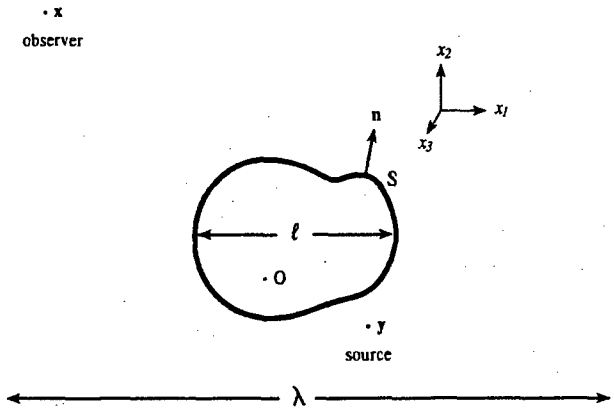

Figure 1

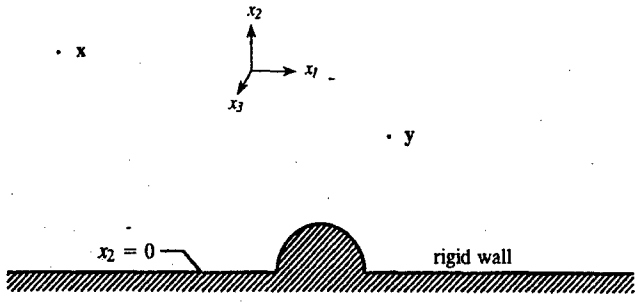

Figure 2

3.2 Surface irregularity This case involves turbulence sources adjacent to a surface that is *locally plane* on the scale of the acoustic wavelength except for the presence of one or more acoustically compact surface irregularities (Figure 2). The Green's function incorporates 'images' of all dipole sources 'in' the wall, such that the net *normal* dipole strength vanishes identically. If the wall coincides with $x_2 = 0$, with fluid in $x_2 > 0$, then

$$G(\mathbf{x},\mathbf{y},t-\tau) = \frac{1}{4\pi|\mathbf{X}-\mathbf{Y}|}\delta\left(t-\tau-\frac{|\mathbf{X}-\mathbf{Y}|}{c_o}\right) + \frac{1}{4\pi|\bar{\mathbf{X}}-\mathbf{Y}|}\delta\left(t-\tau-\frac{|\bar{\mathbf{X}}-\mathbf{Y}|}{c_o}\right), \qquad (3.2)$$

where

$$\left.\begin{aligned} Y_1 &= y_1 - \varphi_1^*(\mathbf{y}), \quad Y_2 = y_2, \quad Y_3 = y_3 - \varphi_3^*(\mathbf{y}) \\ X_1 &= x_1 - \varphi_1^*(\mathbf{x}), \quad X_2 = x_2, \quad X_3 = x_3 - \varphi_3^*(\mathbf{x}) \end{aligned}\right\} \tag{3.3}$$

and $\bar{\mathbf{X}} = (X_1, -X_2, X_3)$. The case of a two-dimensional surface irregularity (projection or cavity) uniform in, say, the x_3-direction is obtained by setting $Y_3 = y_3$, $X_3 = x_3$.

3.3. Radiation from a stationary compact body: vortex interacting with a sphere To evaluate (2.3) take the coordinate origin within S and consider an observer at $\mathbf{x}$ in the acoustic far field ($|\mathbf{x}| \to \infty$). Expand the compact Green's function G to first (*dipole*) order in the retarded time $\mathbf{x}\cdot\mathbf{Y}/c_o|\mathbf{x}|$:

$$\begin{aligned} G(\mathbf{x},\mathbf{y},t-\tau) &= \frac{1}{4\pi|\mathbf{X}-\mathbf{Y}|}\delta\left(t-\tau-\frac{|\mathbf{X}-\mathbf{Y}|}{c_o}\right) \\ &\approx \frac{1}{4\pi|\mathbf{x}|}\delta\left(t-\tau-\frac{|\mathbf{x}|}{c_o}\right) + \frac{x_jY_j}{4\pi c_o|\mathbf{x}|^2}\delta'\left(t-\tau-\frac{|\mathbf{x}|}{c_o}\right), \end{aligned} \tag{3.4}$$

where the prime denotes differentiation with respect to t. The first δ-function is independent of $\mathbf{y}$ and makes no contribution to (2.3), which becomes

$$p(\mathbf{x},t) \approx \frac{-\rho_o x_j}{4\pi c_o|\mathbf{x}|^2}\frac{\partial}{\partial t}\int(\boldsymbol{\omega}\wedge\mathbf{v})\left(\mathbf{y},t-\frac{|\mathbf{x}|}{c_o}\right)\cdot\nabla Y_j(\mathbf{y})d^3\mathbf{y}, \quad |\mathbf{x}|\to\infty. \tag{3.5}$$

The integral represents the retarded dipole strength produced by normal stresses on S. Indeed, the component F_j of the unsteady force exerted by the body on the fluid is given (for incompressible flow) by [3]

$$F_j = -\rho_o\int\boldsymbol{\omega}\wedge\mathbf{v}\cdot\nabla Y_j d^3\mathbf{y} - \eta\oint_{\mathrm{S}}\nabla Y_j\cdot\boldsymbol{\omega}\wedge d\mathbf{S}, \quad \eta=\rho_o\nu, \tag{3.6}$$

where the second, *frictional* component of force can be discarded at very large Reynolds numbers.

To illustrate the procedure consider the sound produced when a line vortex of strength Γ convects past a fixed, rigid sphere. Let the sphere have radius a with center at the coordinate origin, and let the vortex be initially far upstream of the sphere and parallel to the x_3-axis at a distance h above the plane of symmetry $x_2 = 0$ (Figure 3). There is a mean *irrotational* flow in the x_1-direction at speed U, which at sufficiently low Mach number ($M = U/c_o$) is given by

$$\mathbf{U} = U\nabla X_1(\mathbf{x}), \tag{3.7}$$

where $X_1(\mathbf{x})$ is given in the first row of Table 1. The vortex is convected towards the sphere by the mean flow and deformed as it passes around the sphere; more distant parts of the vortex (at $|x_3| \gg a$) are unaffected and remain parallel to the x_3-direction. Figure 3 illustrates the distorted vortex at several values of $T = Ut/a$, when $h/a = 0.2$ and when the self-induced motion of the vortex is neglected.

When surface viscous effects and vortex shedding are ignored, the sound generated during the interaction is given by (3.5) in which $\boldsymbol{\omega}$ is approximated by the vorticity of the distorted line vortex. There is no contribution from unsteady 'drag' ($j = 1$) because $\mathbf{v} = U\nabla Y_1$ and $\boldsymbol{\omega}\wedge\nabla Y_1\cdot\nabla Y_1 \equiv \mathbf{0}$. Similarly, there can be no net 'side-force' on the sphere because of the symmetric shape of the

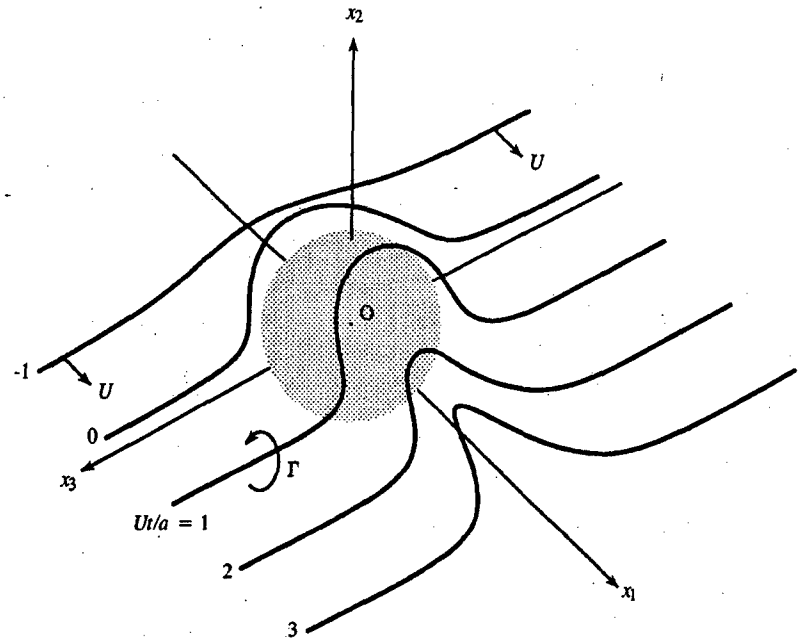

Figure 3

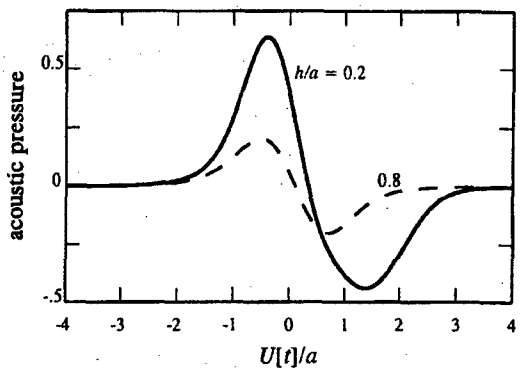

Figure 4

deformed vortex, and therefore there will be no contribution from $j = 3$. The sound is accordingly produced by a dipole orientated in the x_2-direction; i.e. the interaction produces an unsteady 'lift' in this direction which is responsible for the sound, and which can therefore be cast in the form

$$p(\mathbf{x},t) \approx \frac{-\rho_o U \cos\Theta}{4\pi c_o|\mathbf{x}|}\frac{\partial}{\partial t}\int(\boldsymbol{\omega}\cdot\nabla Y_1 \wedge \nabla Y_2)\left(\mathbf{y}, t-\frac{|\mathbf{x}|}{c_o}\right)d^3\mathbf{y}, \quad |\mathbf{x}|\to\infty, \tag{3.8}$$

where $\Theta = \cos^{-1}(x_2/|\mathbf{x}|)$ is the angle between the observer direction $\mathbf{x}$ and the x_2-axis.

Typical plots of the nondimensional pressure

$$\frac{p(\mathbf{x},t)}{\rho_o \Gamma U M \cos\Theta \big/ 4\pi|\mathbf{x}|}$$

are shown plotted against $U[t]/a$ in Figure 4 for two values of h/a; they illustrate how the sound level decreases as the initial standoff distance h of the vortex increases.

In this calculation the unsteady interaction has been evaluated in a linearized approximation, when the unsteady drag is predicted to vanish. Thus, if the sphere is 'stuck' to a plane wall in the presence of a turbulent flow, the present approximation would yield no 'dipole' sound, since only the drag and side force can then make a finite dipole contribution because (from (3.2))

$$G(\mathbf{x},\mathbf{y},t-\tau) \approx \frac{1}{2\pi|\mathbf{x}|}\delta\left(t-\tau-\frac{|\mathbf{x}|}{c_o}\right) + \frac{x_1Y_1 + x_3Y_3}{2\pi c_o|\mathbf{x}|^2}\delta'\left(t-\tau-\frac{|\mathbf{x}|}{c_o}\right). \tag{3.9}$$

3.4. Parallel blade-vortex interactions The same method of solution in terms of the compact Green's function is applicable to airfoils of compact chord and arbitrary span, but it is sufficient here to give explicit results when the span is compact.

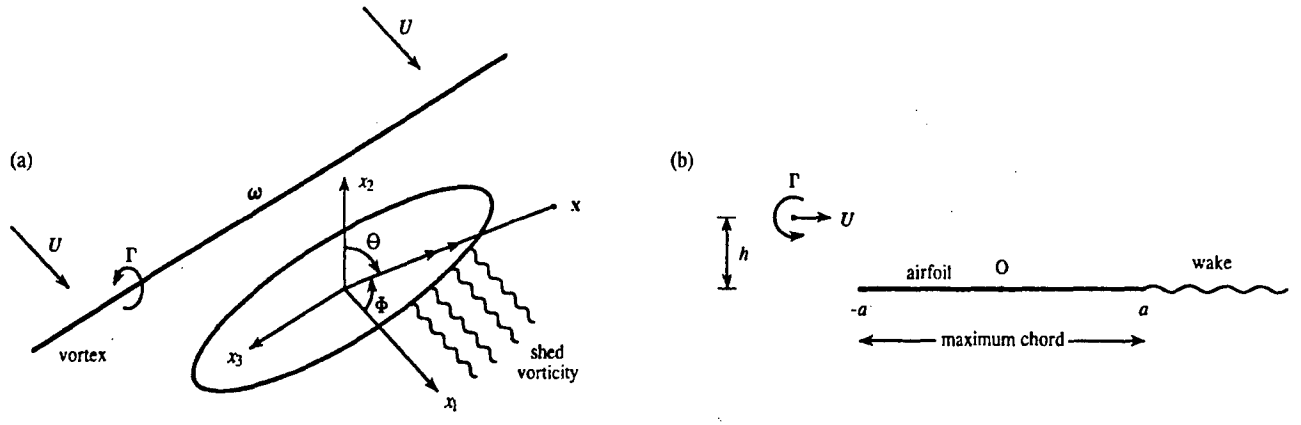

Figure 5

Consider a planar airfoil of rectangular or elliptic planform, orientated as illustrated in Figure 5 at zero angle of attack to a mean flow at speed U in the x_1-direction. A spanwise line vortex of strength Γ is swept past the airfoil at an initial standoff distance h above the airfoil, as indicated in the side view. For an airfoil of compact chord the acoustic pressure produced by the interaction is given by equation (3.5) where, for an airfoil of span L (between $-\frac{1}{2}L < x_3 < \frac{1}{2}L$),

$$Y_1 = y_1, \quad Y_2 = \begin{cases} \mathrm{Re}\big(-i\sqrt{z^2 - \hat{a}(y_3)^2}\big), & |y_3| < \frac{1}{2}L \\ y_2, & |y_3| > \frac{1}{2}L \end{cases}, \quad Y_3 = y_3, \quad z = y_1 + iy_2,$$

where $2\hat{a}(y_3)$ is the airfoil chord at the spanwise location y_3. For the rectangular airfoil $\hat{a}(y_3) \equiv a =$ constant; for the elliptic airfoil we set

$$\frac{\hat{a}(y_3)}{a} = \sqrt{1 - \frac{4y_3^2}{L^2}}, \quad |y_3| < \frac{1}{2}L. \tag{3.10}$$

Vorticity will be shed into the wake of the airfoil in accordance with the Kutta condition. This smooths out conditions at the trailing edge, so that sound is generated primarily by the interaction of the vortex with the leading edge. This is accounted for by removing the trailing edge singularity of the Green's function, by modifying the x_2-component of $\mathbf{Y}$ as follows:

$$Y_2 = \mathrm{Re}\Big(\sqrt{2\hat{a}(y_3)}\sqrt{z + \hat{a}(y_3)}\Big), \quad |y_3| < \frac{1}{2}L. \tag{3.11}$$

In the linearized approximation $\mathbf{v} = (U, 0, 0)$ in (3.5), and the line vortex remains rectilinear; the radiation is produced entirely by the lift dipole. If the vortex crosses the midchord of the airfoil at time $t = 0$, (3.5) yields

$$\frac{p(\mathbf{x}, t)}{\rho_o \Gamma U M \cos\Theta (L/|\mathbf{x}|)/4\pi a} \approx -\frac{1}{2^{\frac{3}{2}}} \int_{-\frac{1}{2}}^{\frac{1}{2}} \mathrm{Im}\left(\frac{\sqrt{\frac{\hat{a}}{a}}}{\left(\frac{U[t]}{a} + \frac{\hat{a}}{a} + i\frac{h}{a}\right)^{\frac{3}{2}}} \right) d\hat{y}_3, \quad M = \frac{U}{c_o}, \tag{3.12}$$

where $\hat{y}_3 = y_3/L$. For a rectangular airfoil the right hand side evaluates to

$$-\frac{1}{2^{\frac{3}{2}}}\mathrm{Im}\left(\frac{1}{\left(\frac{U[t]}{a}+1+i\frac{h}{a}\right)^{\frac{3}{2}}}\right).$$

The acoustic pressure signatures (the left hand side of (3.12)) for the rectangular and elliptic airfoils are plotted in Figure 6 for a vortex standoff distance $h/a = 0.2$. For the rectangular airfoil, the peak amplitude is larger and the width of the acoustic pulse is narrower than for the elliptic airfoil, where the interaction of the leading edge with the vortex occurs over a longer time period.

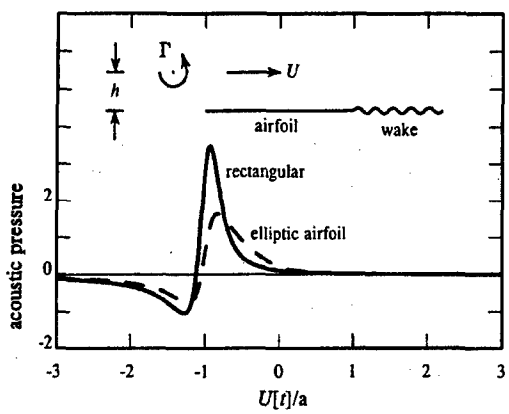

Figure 6

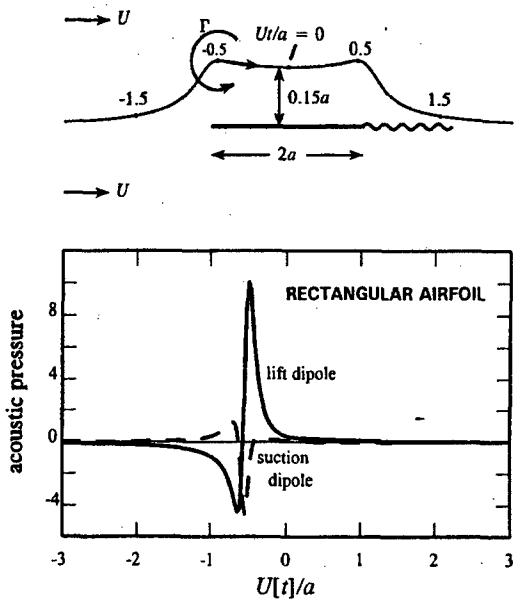

Figure 7

When the $h = 0$ 'image' vorticity in the airfoil prevents the vortex from impinging on the leading edge, and causes the trajectory to be locally deflected above the airfoil (for $\Gamma > 0$). For a rectangular airfoil this case can be treated by assuming that the section of the vortex within the span $-\frac{1}{2}L < x_3 < \frac{1}{2}L$ follows a path that is approximately the same as for locally two-dimensional flow, and by neglecting small contributions from the ends of the airfoil. There are now two distinct dipole components of the sound: that discussed above (p_2, say) associated with the unsteady lift, and a second smaller component (p_1) produced by the unsteady 'suction' force' at the leading edge. The corresponding nondimensional pressures

$$\frac{p_1(\mathbf{x},t)}{\rho_o\Gamma UM\cos\Phi(L/|\mathbf{x}|)/4\pi a}, \qquad \frac{p_2(\mathbf{x},t)}{\rho_o\Gamma UM\cos\Theta(L/|\mathbf{x}|)/4\pi a}$$

are plotted in Figure 7 for a velocity ratio $\Gamma/4\pi aU = 0.2$. The upper part of the figure shows the path followed by those sections of the vortex inboard of the airfoil tips.

4. NONCOMPACT BODIES

4.1 Edge noise Our discussion will be framed in terms of the canonical, parallel-sided airfoil shape illustrated schematically in Figure 8, which has chord ℓ and uniform thickness h, and a rounded nose. Take the origin O at a convenient point near the trailing edge such that the 'upper' and 'lower' planar surfaces of the airfoil are at $x_2 = \pm\frac{1}{2}h$, the x_1-axis is in the direction of the mean flow, and x_3 is parallel to the airfoil span (out of the plane of the paper in Figure 8a).

When these conditions are satisfied the far field acoustic pressure fluctuations $p(\mathbf{x},\omega)e^{-i\omega t}$ of frequency ω produced by the interaction of the turbulence with the airfoil are given by the following form of (3.5)

$$p(\mathbf{x},\omega) = \rho_0 \int \frac{\partial G}{\partial \mathbf{y}}(\mathbf{x},\mathbf{y},\omega) \cdot \big(\omega \wedge \mathbf{v}\big)(\mathbf{y},\omega) d^3\mathbf{y}, \tag{4.1}$$

where $G(\mathbf{x},\mathbf{y},\omega)$ is the *time harmonic* Green's function, which satisfies $G(\mathbf{x},\mathbf{y},t-\tau) = \frac{-1}{2\pi}\int_{-\infty}^{\infty} G(\mathbf{x},\mathbf{y},\omega)e^{-i\omega(t-\tau)}d\omega$.

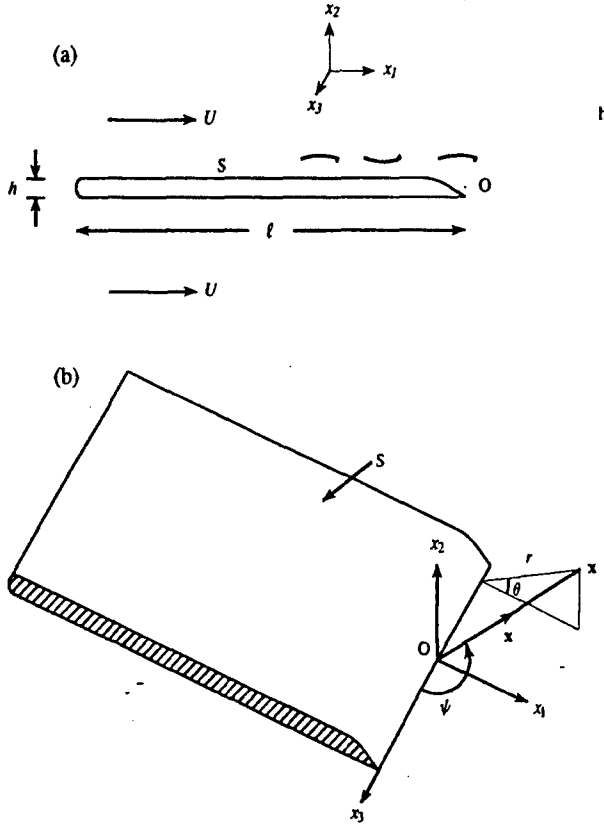

Figure 8

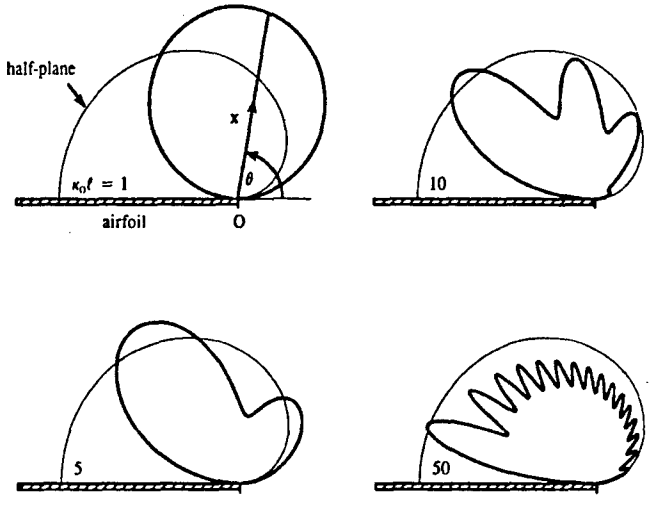

Figure 9

At low Mach numbers the trailing edge noise is dominated by contributions to (4.1) from the neighborhood of the edge. The wavelength of the sound $\sim \delta/M$, where δ is a length that characterizes the eddy size near the edge, and may in practice be of the order of the boundary layer thickness or the airfoil thickness h. In either case the acoustic wavelength greatly exceeds h when $M \ll 1$, which implies that the turbulence responsible for the edge noise is always very

much closer than an acoustic wavelength from the edge. Then the nondimensional source distance $\kappa_o\sqrt{y_1^2+y_2^2} \sim \sqrt{y_1^2+y_2^2}/\text{acoustic wavelength} \ll 1$, where $\kappa_o = \omega/c_o$ is the acoustic wavenumber. When the observation point $\mathbf{x}$ is in the acoustic far field and $\mathbf{y}$ is within the source region, Green's function can be expanded in terms of this small parameter. When the airfoil chord ℓ is noncompact ($\kappa_o\ell \gg 1$), the first nontrivial term in this expansion yields

$$G(\mathbf{x},\mathbf{y},\omega) \approx \frac{-\sqrt{\kappa_o}\sin^{\frac{1}{2}}\psi \sin\left(\frac{\theta}{2}\right)\varphi^*(\mathbf{y})e^{i\kappa_o|\mathbf{x}-y_3\mathbf{i}_3|}}{\pi\sqrt{2\pi i}|\mathbf{x}-y_3\mathbf{i}_3|}, \quad \kappa_o\ell \to \infty, \quad \kappa_o\sqrt{y_1^2+y_2^2} \ll 1. \tag{4.2}$$

where $\mathbf{i}_3$ is a unit vector parallel to the airfoil span (in the positive x_3-direction). If $r = \sqrt{x_1^2+x_2^2}$ denotes the observer distance from the edge of the airfoil ($\sim$ the x_3-axis), then (r,θ) are the polar coordinates of the observer position relative to a plane $x_3 =$ constant, i.e. $(x_1,x_2) = r(\cos\theta,\sin\theta)$; $\psi = \sin^{-1}(r/|\mathbf{x}|)$ is the angle between the observer direction $\mathbf{x}$ and the edge (see Figure 8b). The function $\varphi^*(\mathbf{y}) \equiv \varphi^*(y_1,y_2)$ of the source position $\mathbf{y}$ is the velocity potential of ideal, incompressible flow around the edge (in the anticlockwise direction), and therefore depends on the geometrical shape of the edge. At source distances $\sqrt{y_1^2+y_2^2}$ from the edge that are large compared to the airfoil thickness h but small compared to the chord ℓ, $\varphi^*(\mathbf{y})$ must tend to the following expression for the potential of flow around a rigid *half-plane*:

$$\varphi^*(\mathbf{y}) \to \sqrt{r'}\sin(\theta'/2), \quad h \ll r' \ll \ell, \quad \text{where } (y_1,y_2) = r'(\cos\theta',\sin\theta'). \tag{4.3}$$

In applications where the wavelength is not necessarily small compared to the chord ℓ the representation (4.2) is modified in its dependence on frequency and on the directivity, but the edge potential function $\varphi^*(\mathbf{y})$ is unchanged. This is illustrated in Figure 9 [6] for $\psi = 90°$ and $\kappa_o\ell = 1,\ 5,\ 10$ and 50. The heavy curves are polar plots of the *linear* pressure amplitude (normalized to the same maximum value); in each case the light curve corresponds to the $\sin\left(\frac{\theta}{2}\right)$ directionality for $\kappa_o\ell = \infty$. At the lowest frequency shown in Figure 9 ($\kappa_o\ell = 1$) the radiation peaks in directions normal to the airfoil, and the directivity coincides with that for a *dipole* source orientated in the x_2-direction (as for the compact chord airfoil of §3.4). Multiple lobes develop as the frequency increases, and the directivity tends in an oscillatory manner towards that for the semi-infinite airfoil. In all cases there are radiation nulls in the directions $\theta = 0°$ and 180°, respectively downstream and upstream of the airfoil.

The above argument implies that the influence of finite chord on the trailing edge noise frequency spectrum does not depend on the edge geometry. In Figure 10 we compare the predicted edge noise spectra for a semi-infinite airfoil with that for an airfoil of finite chord ℓ for two different radiation directions, and for the following parameter values that are typical of model scale tests conducted in air and in associated numerical simulations [7 - 13]

$$\frac{\ell}{\delta_*} \approx 78, \quad M = 0.09, \tag{4.4}$$

where δ_* is the boundary layer displacement thickness in the vicinity of the trailing edge. Significant departures from the half-plane prediction occur for $\omega\delta_*/U < 0.4$; in particular spectral levels are much reduced at frequencies below that of the spectral peak, which is shifted to higher frequencies.

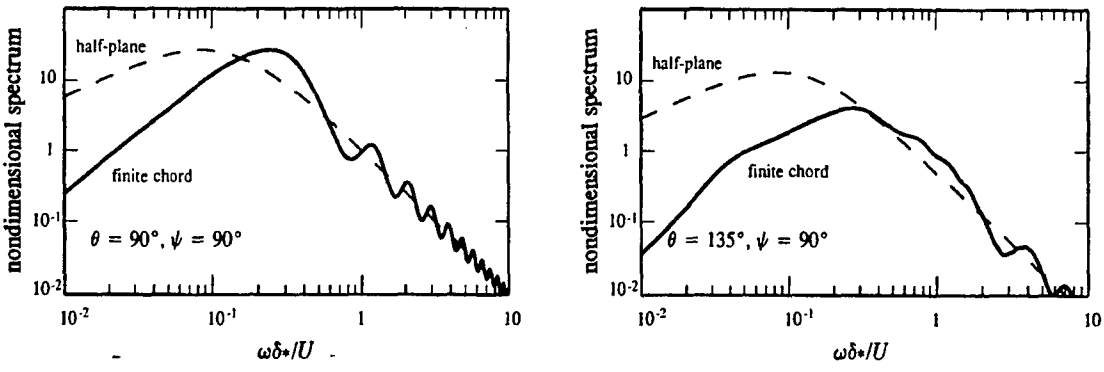

Figure 10

4.2 Projectile entering a duct The overall pressure rise across the compression wave produced ahead of a bullet shaped body projected into a long, but finite duct of cross-sectional area $\mathcal{A} = \pi R^2$ fitted with a long, cylindrical entrance 'hood' of length ℓ_h and cross-section $\mathcal{A}_h = \pi R_h^2$ (Figure 11) is given approximately by [14]

$$\Delta p = \frac{\rho_o U^2}{(1-M^2)} \frac{\mathcal{A}_o}{\mathcal{A}} \left(1 + \frac{\mathcal{A}_o}{\mathcal{A}}\right), \tag{4.5}$$

where U and $\mathcal{A}_o$ respectively denote the projection speed and the cross-sectional area of the body, and $M = U/c_o$.

When the blockage $\mathcal{A}_o/\mathcal{A}$ is small and the projection Mach number M does not exceed about 0.4, the initial form of the compression wave can be calculated from the following modified form of (1.2):

$$\left(\frac{1}{c_o^2}\frac{\partial^2}{\partial t^2} - \nabla^2\right) B = \frac{U}{(1-M^2)} \left(1 + \frac{\mathcal{A}_o}{\mathcal{A}}\right) \frac{\partial}{\partial t} \left(\frac{\partial \mathcal{A}_T}{\partial x_1}(x_1 + Ut)\delta(x_2)\delta(x_3)\right) + \mathrm{div}(\omega \wedge \mathbf{v}), \tag{4.6}$$

The new source term is a slender body representation of the body, which is assumed to travel along the axis of the duct (the negative x_1-axis), where $\mathcal{A}_T(s)$ is the body cross-sectional area at distance s *from the tip of the nose*, which is taken to cross the entrance plane of the hood at time $t = 0$.

The characteristic wavelength of the sound produced when the body interacts with the duct entrance is sufficiently large ($\sim R_h/M$) that only plane waves can propagate into the duct. The corresponding compact Green's function for an observer at $\mathbf{x}$ deep inside the duct then has the form

$$G(\mathbf{x},\mathbf{y};t-\tau) \;=\; \frac{c_o \mathcal{T}_J}{2\mathcal{A}_h} \sum_{n=0}^{\infty} \mathcal{R}_E^n \mathcal{R}_J^n \left\{ \mathrm{H}\left([t] - \tau - \frac{(2n\ell + \varphi^*(\mathbf{y}))}{c_o}\right) + \mathcal{R}_E \mathrm{H}\left([t] - \tau - \frac{(2n\ell - \varphi^*(\mathbf{y}))}{c_o}\right)\right\}$$

$$x_1 \to -\infty, \tag{4.7}$$

where $[t] = t + (x_1 - \ell')/c_o$ is the retarded time ($\ell' \approx 0.61 R_h$ being the 'end correction' of the hood entrance [15]). The velocity potential $\varphi^*(\mathbf{x})$ represents an irrotational, incompressible flow *out* of

the hood from $x_1 = -\infty$, normalized such that

$$\begin{aligned} \varphi^*(\mathbf{x}) &\sim x_1 - \ell' \quad \text{when} \quad |x_1| \gg R_h \quad \text{within the hood,} \\ &\sim \frac{-\mathcal{A}_h}{4\pi|\mathbf{x}|} \quad \text{when} \quad |\mathbf{x}| \gg R_h \quad \text{outside the hood.} \end{aligned} \tag{4.8}$$

Also,

$$\mathcal{R}_{\mathrm{E}} = -1, \quad \mathcal{R}_{\mathrm{J}} = \frac{\mathcal{A}_h - \mathcal{A}}{\mathcal{A}_h + \mathcal{A}}, \quad \mathcal{T}_{\mathrm{J}} = \frac{2\mathcal{A}_h}{\mathcal{A}_h + \mathcal{A}}. \tag{4.9}$$

$\mathcal{R}_{\mathrm{E}}$ is the reflection coefficient for long sound waves at the open end; $\mathcal{R}_{\mathrm{J}}$ is the reflection coefficient at the junction of the hood and uniform duct for reflection *back into* the hood; and $\mathcal{T}_{\mathrm{J}}$ is the transmission coefficient for transmission from the hood into the duct. Formula (4.7) is uniformly valid for source positions $\mathbf{y}$ lying within the hood and the neighborhood of its ends.

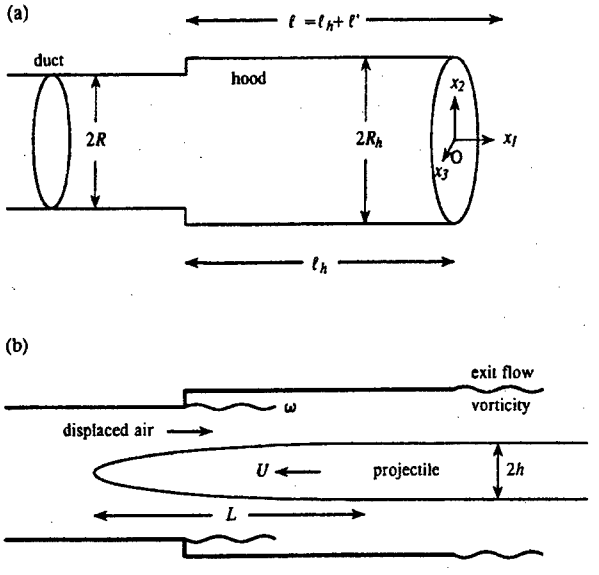

Figure 11

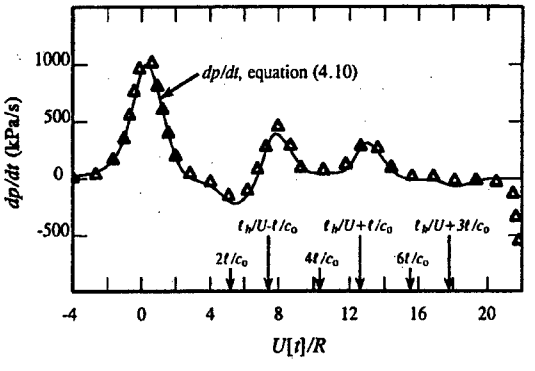

Figure 12

To understand the terms in the brace brackets of (4.7), consider the case where the source point $\mathbf{y}$ lies in the body of the hood. For $n = 0$ the first Heaviside function represents the front of the disturbance radiated into the duct; the second is the contribution from the wavefront that initially propagates towards the hood entrance, where it is reflected with reflection coefficient $\mathcal{R}_{\mathrm{E}} = -1$ and subsequently transmitted into the duct; the amplitude of each of these 'direct' waves is *increased* on transmission through the junction into the duct because the transmission coefficient $\mathcal{T}_{\mathrm{J}} > 1$. The terms in $n \geq 1$ represent contributions arriving at later times, after the transmission into the duct of those components of the direct waves that have suffered n reflections from both ends of the hood; the amplitude decreases by a factor $\mathcal{R}_{\mathrm{J}} < 1$ on each reflection back into the hood from the junction with the duct, so that the higher order modes rapidly decrease in amplitude.

The amplitude and profile of the sound wave radiated from the far end of the duct when the compression wave arrives is proportional to the compression wave pressure 'gradient' $\partial p/\partial t$

incident on the exit. The *linear theory* prediction of $\partial p/\partial t$ is given by the solution of (4.6) in terms of the Green's function (4.7). In a long duct it would also be necessary to account for nonlinear steepening of the compression wave; the solution of (4.6) should therefore be regarded as providing the *initial conditions* for such a nonlinear calculation.

The principal source of the compression wave is the monopole representing displacement of fluid by the nose of the projectile and a dipole generated by the drag produced by the pressure rise over the nose, both of which are accounted for by the first term on the right of (4.6) [14]. The vortex source represents secondary effects of separation on the body, on the duct walls, and in the shear layers of the 'exit' flows from the hood mouth and through the junction from the duct into the hood, of the fluid displaced by the entering projectile. The contribution from the monopole and dipole can be written

$$\frac{\partial p}{\partial t} = \frac{\rho_o U^3}{(1-M^2)}\left(1+\frac{\mathcal{A}_o}{\mathcal{A}}\right)\iint_{-\infty}^{\infty}\frac{\partial \mathcal{A}_T}{\partial y_1}(y_1+U\tau)\frac{\partial^2 G}{\partial y_1^2}(\mathbf{x},y_1,0,0;t-\tau)dy_1 d\tau. \tag{4.10}$$

Figure 12 illustrates a comparison of this solution with an experiment in air using a 7 m long horizontal, unflanged, circular cylindrical duct made of hard vinyl chloride, with inner radius $R =$ 5 cm. An axisymmetric body is projected into the duct, guided by a 5 mm diameter taut steel wire extending along the duct axis. Pressure measurements are made using a wall-mounted transducer 1.5 m from the hood entrance. The hood consists of a circular cylindrical, vinyl chloride pipe of inner radius $R_h = 6.25$ cm; therefore $\mathcal{A}_h/\mathcal{A} \equiv R_h^2/R^2 = 1.5625$. A 10 cm collar at one end of the hood facilitates an airtight and smooth mating with the duct. When in place the hood has an overall length of 60.3 cm, and a 'working length' of $\ell_h = 50$ cm.

The projectile had an ellipsoidal nose profile obtained by rotating the curve $y = h\sqrt{(x/L)(2-x/L)}$, $0 < x < L$ about the x-axis, so that

$$\frac{\mathcal{A}_T(x)}{\mathcal{A}_o} = \begin{cases} \frac{x}{L}\left(2-\frac{x}{L}\right), & 0<x<L, \\ 1, & x>L, \end{cases} \quad \text{where } h = 2.235\,\text{cm} \quad L = 11.18\,\text{cm}, \tag{4.11}$$

and $\mathcal{A}_o = \pi h^2$. The model had overall length equal to 124.3 cm, and fore-aft symmetry with equal nose and tail profiles

The solid curve in Figure 12 is the prediction of equations (4.7), (4.10) for $U = 294$ kph ($M = 0.24$), plotted as a function of the non-dimensional retarded time $U[t]/R$, where the nose of the projectile crosses the entrance plane of the hood at $t = 0$. The open triangles are observed values of the pressure gradient measured in the duct at a distance of 1.5 m from the entrance plane of the hood. The agreement between theory and experiment is excellent; the wavy nature of the pressure gradient profile is caused by interference between waves multiply reflected (temporarily trapped) within the hood before transmission into the duct. The theory based on (4.7) is seen to capture this interference perfectly.

REFERENCES

1. M. J. Lighthill 1952 On sound generated aerodynamically. Part I: General theory. *Proc. Roy. Soc. Lond.* **A211**, 564 - 587.
2. M. S. Howe 1975 Contributions to the theory of aerodynamic sound, with application to excess jet noise and the theory of the flute. *J. Fluid Mech.* **71**, 625 - 673.
3. M. S. Howe 1998 *Acoustics of Fluid-Structure Interactions*, Cambridge University Press.
4. L. D. Landau and E. M. Lifshitz 1987 *Fluid Mechanics* (Second edition). Oxford: Pergamon.
5. D. G. Crighton, A. P. Dowling, J. E. Ffowcs Williams, M. Heckl and F. G. Leppington 1992 *Modern Methods in Analytical Acoustics (Lecture Notes)*. Springer-Verlag: London.
6. M. S. Howe 2001 Edge-source acoustic Green's function for an airfoil of arbitrary chord, with application to trailing edge noise. *Q. J. Mech. and Appl. Math.* **54**, 139 - 155.
7. W. K. Blake 1986 *Mechanics of flow-induced sound and vibration*, Vol. 2: *Complex flow-structure interactions*. New York: Academic Press.
8. J. Gershfeld, W. K. Blake and C. W. Knisely 1988 *AIAA Paper* 88-3826-CP Trailing edge flow and aerodynamic sound.
9. W. K. Blake and J. L. Gershfeld 1989 in *Lecture Notes in Engineering* 46 (Ed. M. Gad-el-Hak). Frontiers in Experimental Fluid Mechanics: The aeroacoustics of trailing edges.
10. T. F. Brooks, D. S. Pope and M. A. Marcolini 1989 *National Aeronautics and Space Administration Reference Publication No. 1218.* Airfoil self-noise and prediction.
11. M. Wang 1997 *Annual Research Briefs* 37 - 49, (Center for Turbulence Research, Stanford University). Progress in large-eddy simulation of trailing-edge turbulence and aeroacoustics.
12. M. Wang 1998 *Annual Research Briefs* 91 -106, (Center for Turbulence Research, Stanford University). Computation of trailing-edge noise at low mach number using LES and acoustic analogy.
13. M. Wang and P. Moin 1999 Submitted to *AIAA J.* Computation of trailing-edge noise using large-eddy simulation.
14. M. S. Howe, M. Iida, T. Fukuda and T. Maeda 2000 Theoretical and experimental investigation of the compression wave generated by a train entering a tunnel with a flared portal *J. Fluid Mech.* **425**, 111 - 132.
15. Lord Rayleigh 1926 *The Theory of Sound*, Volume 2. London: Macmillan.